Inorganic Chemistry

Article

pubs.acs.org/IC

Three-Dimensional (3-D) Ferromagnetic Network of Mn_{12} Single-Molecule Magnets: Subtle Environmental Effects and Switching to Antiferromagnetic

Adeline D. Fournet,[†,§] Kylie J. Mitchell,[†] Wolfgang Wernsdorfer,[‡] Khalil A. Abboud,[†] and George Christou*[,†]

[†]Department of Chemistry, University of Florida, Gainesville, Florida 32611, United States

[‡]Institut Néel-CNRS and University Grenoble Alpes, F-38000 Grenoble, Cedex 9, France

Supporting Information

ABSTRACT: A new member of the Mn_{12} family of single-molecule magnets (SMMs) has been prepared and found to be the first of this family to give a 3-D ferromagnetic network. $[Mn_{12}O_{12}(O_2CC_6H_4\text{-}p\text{-}F)_{16}(H_2O)_4]$ (**2**) was prepared by carboxylate substitution on the acetate derivative with *p*-F-benzoic acid and crystallizes as **2**·8MeCN in space group $I\bar{4}2m$ with extensive formation of intermolecular C−H···F hydrogen-bonding. The latter leads to a combination of ferromagnetic (F) and antiferromagnetic (AF) interactions and an overall F network that gives a $\chi_M T$ value at low T that is abnormally high for an $S = 10$ ground state. **2**·8MeCN undergoes solvent loss under vacuum to **2**, with a decrease in unit-cell volume of 17%, primarily due to a 13% decrease in the *c*-axis. The $\chi_M T$ vs T plot for **2** indicates a switch to a net AF network. Exposure to air causes hydration to **2**·3H_2O, a concomitant increase in unit cell volume, and a switch back to a F network. The same conversion of **2**·8MeCN to **2**·3H_2O can also be accomplished in one step rather than two steps, by leaving crystals of the former exposed to air at ambient temperature and pressure for 10 days, giving the same magnetic plots. Interestingly, the desolvation/solvation processes cause Jahn−Teller isomerism to occur, but the ratio of the faster-relaxing isomer to the normal slowly relaxing one does not change monotonically. Single-crystal micro-SQUID studies on **2**·8MeCN show the expected magnetization hysteresis loops for a SMM and a small exchange-bias from the intermolecular interactions that is unexpectedly AF. Since the micro-SQUID study only identifies interactions along the easy-axis (*z*-axis) of the crystal, this is readily rationalized as due to the J_z components of the intermolecular interactions in **2**·8MeCN being net AF. The combined results offer useful insights into the degree of sensitivity of the magnetic properties to small environmental perturbations.

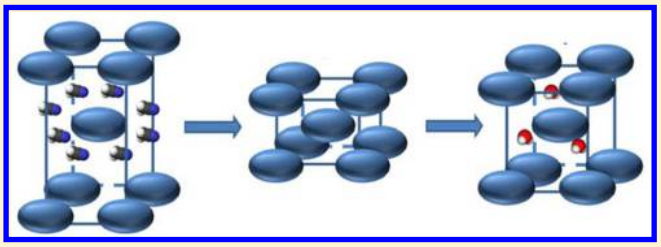

INTRODUCTION

The $[Mn_{12}O_{12}(O_2CR)_{16}(H_2O)_4]$ family of prototypical single-molecule magnets (SMMs) have been known since the synthesis and preliminary magnetic properties of the R = Me member were reported in 1980 by Lis.[1] These Mn_{12} clusters have since become the most well-studied and best understood SMMs and, thus, the source of a large fraction of our current knowledge of this fascinating magnetic phenomenon.[2−4] In addition, the number and variety of SMMs have expanded dramatically in the last two decades or so, and currently includes various d/d and d/f mixed-metal combinations, the more recent activity in homometallic lanthanide[5] and actinide chemistry,[6,7] as well as mononuclear 3d SMMs.[8] This field now represents a well-established, deep-rooted, bottom-up approach to nanoscale magnetism, retaining all the advantages of molecular chemistry, such as monodispersity, solubility, organic ligation, and crystallinity. The latter has been of particular importance in providing (i) structural information to atomic precision via single-crystal X-ray crystallography, and (ii) ordered assemblies of identically oriented SMMs whose study has allowed various fragile and nebulous quantum effects to be discovered, often using members of the Mn_{12} family.[9−11]

Over the years, we have reported on a variety of ways of modifying the Mn_{12} (and other) SMMs, which has allowed the assessment of how many important properties of the clusters are affected by the nature of the carboxylate or other ligands, the cluster oxidation state, the crystal site symmetry, small structural modifications to the core, and others. As a result, a large database of knowledge is now available. Even after all these years, however, only recently has a three-dimensional (3-D) network of Mn_{12} molecules been prepared with significant intermolecular hydrogen-bonding interactions directly between Mn_{12} molecules rather than to or through lattice solvent molecules. Thus, $[Mn_{12}O_{12}(O_2CMe)_{12}(NO_3)_4(H_2O)_4]$ contains O−H···O hydrogen bonds between water and nitrate ligands on adjacent Mn_{12} molecules.[12] Therefore, as described

Received: June 30, 2017
Published: August 22, 2017

DOI: 10.1021/acs.inorgchem.7b01676
Inorg. Chem. 2017, 56, 10706−10716

elsewhere, this complex crystallizes as a 3-D antiferromagnetic (AF) network.[13]

Situations in which neighboring SMM units are exchange-coupled, whether they be dimers or any other oligomeric assembly through to 3-D networks, offer the opportunity to observe exchange-biased quantum tunneling of magnetization (QTM), by which neighboring molecules provide bias fields shifting the QTM steps from their normal positions. One potentially important consequence of this effect is suppression of QTM at zero applied field in SMM dimers.[14] Examples of this phenomenon have been found in compounds with intermolecular interactions mediated by hydrogen bonding[14−19] or covalent linkages.[20−23] Several interesting studies have also been published, showing switching on and/or modulation of SMM properties via external stimuli such as light,[24−26] solvation,[27] or redox changes.[28,29] It was with these latter reports in mind that we were intrigued by a new $[Mn_{12}O_{12}(O_2CR)_{16}(H_2O)_4]$ SMM that we had found to have unprecedented properties, and to undergo changes to those properties upon solvation changes.

We thus describe herein the synthesis, crystal structure, and magnetic properties of a 3-D network of Mn_{12} single-molecule magnets formed from extensive intermolecular C−H···F hydrogen bonding that leads to net ferromagnetic (F) interactions between the Mn_{12} molecules. This unprecedented situation is rationalized by analyzing the different types of C−H···F hydrogen-bonds involving *ortho* vs *meta* C−H positions of the aromatic ring. We also describe the effect on the magnetic properties of crystal-to-crystal changes to the environments of the Mn_{12} molecules caused by the loss and gain of solvent molecules.

EXPERIMENTAL SECTION

Synthesis. All manipulations were performed under aerobic conditions using reagents and solvents as received, unless otherwise stated. $[Mn_{12}O_{12}(O_2CMe)_{16}(H_2O)_4]\cdot 2MeCO_2H\cdot 4H_2O$ (**1**) was prepared as described elsewhere.[1]

$[Mn_{12}O_{12}(O_2CC_6H_4$-*p*-F)$_{16}(H_2O)_4]$ (2). To a stirred solution of **1** (2.00 g, 0.97 mmol) in CH_2Cl_2 (100 mL) was added *para*-fluorobenzoic acid (2.80 g, 20.0 mmol). The resulting solution was stirred overnight and the solvent was removed by rotoevaporation in vacuum. Toluene (25 mL) was added to the residue, and the solution was again rotoevaporated to dryness. The addition and removal of toluene were repeated two more times. The residue was then dissolved in CH_2Cl_2 (50 mL), filtered, layered with MeCN, and left undisturbed for 10 days at room temperature, during which time large black crystals of **2**·8MeCN slowly grew. Crystals were maintained in mother liquor for the X-ray crystallographic analysis; otherwise, they were collected by filtration, washed with MeCN, and dried under vacuum for other solid-state studies. The yield was 75%. Selected IR data (KBr pellet, cm^{-1}): 3424(b), 3125(b), 1698(w), 1604(s), 1570(m), 1507(s), 1416(vs), 1352(s), 1300(w), 1233(s), 1153(s), 1093(m), 1015(m), 857(m), 798(w), 778(s), 712(w), 692(m), 632(sb), 552(m).

Samples vacuum-dried for 2 h and not exposed to air analyzed as solvent-free **2** ($C_{112}H_{72}F_{16}Mn_{12}O_{48}$). Anal. Calcd (Found): C, 42.72% (42.98%); H, 2.30% (2.14%); N, 0.00% (0.00%).

Samples vacuum-dried for 2 h and exposed to air for 32 h or more analyzed as **2**·3H_2O ($C_{112}H_{78}F_{16}Mn_{12}O_{51}$). Anal. Calcd (Found): C, 42.00% (41.71%); H, 2.45% (2.49%); N, 0.00% (0.00%); F, 9.49% (9.63%).

Samples removed from mother liquor, dried with tissue, and maintained in air for 10 days also analyzed as **2**·3H_2O. Anal. Calcd (Found): C, 42.00% (41.80%); H, 2.45% (2.34%); N, 0.00% (0.00%).

X-ray Crystallography. Data were collected on **2**·8MeCN at 100 K on a Bruker DUO diffractometer, using Mo Kα radiation (λ = 0.71073 Å) and an APEXII CCD area detector. Raw data frames were read using the SAINT program[30] and integrated using 3D profiling algorithms. The resulting data were reduced to produce *hkl* reflections and their intensities and estimated standard deviations. The data were corrected for Lorentz and polarization effects, and numerical absorption corrections were applied based on indexed and measured faces.

The structure was solved and refined on F^2 in SHELXTL2013,[30] using full-matrix least-squares cycles of refinement. The non-H atoms were refined with anisotropic thermal parameters, and all H atoms were placed in idealized positions and refined riding on their parent atoms. The asymmetric unit consists of $^1/_8$ of a Mn_{12} cluster on a $\bar{4}2m$ site and one MeCN solvent disordered over two positions. Unfortunately, the high symmetry produces a complicated Mn_{12} structure involving disordered carboxylate groups: (i) The C1 ligands lie in the equatorial plane of the Mn_{12} molecule, and the entire ligand (including its O atoms) is disordered and was refined in two parts with near-parallel planes; (ii) The C11 and C21 ligands are axial, lying above and below the equatorial plane. The C11 ligand has only its C_6H_4F part disordered and was again refined in two parts related to each other by simple reflection. The C21 ligand is disordered about a mirror plane lying on the bisector of the angle formed by three axial O atoms positioned in a row: the carboxylate occupies a pair of them and the third is a water ligand, and its disorder partner has the carboxylate and water positions reversed.

The MeCN molecules were disordered and could not be modeled properly; therefore, the SQUEEZE program,[31] which is part of the PLATON[32] package of crystallographic software, was used to calculate the solvent disorder area and remove its contribution to the overall intensity data. In the final cycle of refinement, 4361 reflections (3436 of which are observed with $I > 2\sigma(I)$) were used to refine 147 parameters, and the resulting R_1, wR_2, and goodness of fit (S) were 5.79%, 15.76%, and 1.076, respectively. Crystal data and structure refinement details are collected in Table 1.

Table 1. Crystal Data and Structure Refinement Parameters for 2·8MeCN

parameter	value
formula[a]	$C_{128}H_{96}F_{16}Mn_{12}N_8O_{48}$
formula weight, fw	3477.40 g mol^{-1}
space group	$I\bar{4}2m$
a	17.4099(12) Å
b	17.4099(12) Å
c	23.8737(17) Å
V	7236.2(11) $Å^3$
Z	2
T	100(2) K
radiation[b]	0.71073 Å
ρ_{calc}	1.596 g cm^{-3}
μ	1.114 mm^{-1}
$R1$[c,d]	0.0579
$wR2$[e]	0.1576

[a]Including solvent molecules. [b]Graphite monochromator. [c]$I > 2\sigma(I)$. [d]$R1 = 100\sum(||F_o| - |F_c||)/\sum|F_o|$. [e]$wR2 = 100[\sum[w(F_o^2 - F_c^2)^2]/\sum[w(F_o^2)^2]]^{1/2}$, $w = 1/[\sum^2(F_o^2) + [(ap)^2 + bp]$, where $p = [\max(F_o^2,0) + 2F_c^2]/3$.

Vacuum-dried crystals of **2**·8MeCN, with or without subsequent exposure to air, retain their crystallinity and still diffract X-rays well enough for unit-cell parameters to be obtained, as do crystals allowed to lose MeCN at ambient pressure and humidity for 10 days. Unit-cell dimensions were obtained for all of these samples.

Other Studies. Infrared spectra were recorded in the solid state (KBr pellets) on a Nicolet Nexus 670 FTIR spectrophotometer in the 400−4000 cm^{-1} range. Elemental analyses were performed by the in-house facilities of the University of Florida Chemistry Department or at Atlantic Microlab, Inc. Magnetic susceptibility studies were

DOI: 10.1021/acs.inorgchem.7b01676
Inorg. Chem. 2017, 56, 10706−10716

performed at the University of Florida on a Quantum Design MPMS-XL SQUID magnetometer that was equipped with a 7 T dc magnet and was capable of operating in the 1.8−400 K range. Pascal's constants were used to estimate the diamagnetic contribution to the susceptibility, which was subtracted from the experimental susceptibility to give the molar magnetic susceptibility (χ_M). Samples were embedded in solid eicosane to prevent torquing, unless otherwise stated. dc susceptibility data were collected in the 5.0−300 K range in a 0.1 T dc field. ac susceptibility data were collected in the 1.8−15 K range in zero dc field and a 3.5 G ac field with oscillation frequencies up to 1500 Hz. Magnetization versus field and temperature data were collected in the 1.8−10.0 K range in dc fields up to 7 T and were fit using the program MAGNET.[33] Magnetization hysteresis studies were carried out using an array of micro-SQUIDs, whose high sensitivity allows the study of single crystals of the order of 10−500 μm. The field can be applied in any direction by separately driving three orthogonal coils.

RESULTS AND DISCUSSION

Synthesis. Complex **2** was prepared from the acetate analogue **1** using the standard carboxylate substitution procedure developed for the Mn_{12} family.[34] Thus, **1** was treated with an excess of p-$FC_6H_4CO_2H$ and the resulting equilibrium driven to completion by the removal of $MeCO_2H$ as its toluene azeotrope (reaction 1, where R = p-FC_6H_4). The product was isolated as **2**·8MeCN in 75% yield as black crystals that would often grow quite large (~5 mm dimensions).

$$[Mn_{12}O_{12}(O_2CMe)_{16}(H_2O)_4] + 16RCO_2H \rightarrow [Mn_{12}O_{12}(O_2CR)_{16}(H_2O)_4] + 16MeCO_2H \quad (1)$$

Description of Structure. Complex **2**·8MeCN crystallizes in space group $I\bar{4}2m$ with the molecules arranged as a body-centered cubic lattice. Therefore, they are oriented identically with parallel z-axes (see Figure S1 in the Supporting Information).[35] The asymmetric unit consists of $^1/_8$ of a Mn_{12} cluster located on a $\bar{4}2m$ position, and one MeCN molecule disordered over two positions. The disklike cluster has the typical structure of the Mn_{12} family, with a central $\{Mn^{IV}_4O_4\}$ cube held within a nonplanar Mn^{III}_8 loop by eight μ_3−O^{2-} ions (see Figure 1). Peripheral ligation is by 16 μ-carboxylate and four terminal H_2O groups, which all exhibit some degree of disorder because of the high crystallographic $\bar{4}2m$ symmetry but lower molecular symmetry (S_4). One component of the disorder is shown in Figure 1, and a more complete representation of the disorder is shown in Figure S2 in the Supporting Information,[35] including the H_2O/carboxylate disorder caused by the mirror planes.

Some additional structural features will be crucial to the discussion of the magnetic properties (vide infra) and are thus described here:

(a) The Mn^{III} Jahn−Teller (JT) elongation axes (black bonds in Figure 1, bottom) are all oriented in the usual way, i.e., avoiding the μ_3-O^{2-} ions and thus near-parallel to the z-axis of the molecule. This is the normal Mn_{12} structure, usually called the slower-relaxing (SR) JT isomer, since it has the larger effective barrier (U_{eff}) to magnetization relaxation. In contrast, the faster-relaxing (FR) JT isomer has a smaller U_{eff} resulting from one JT axis being abnormally oriented, i.e., toward a μ_3−O^{2-} ion and nearly in the equatorial plane of the molecule.[36]

(b) The $\{Mn_{12}O_{12}\}$ core of **2** is essentially superimposable with those of other Mn_{12} analogues, such as **1** and $[Mn_{12}O_{12}(O_2CPh)_{16}(H_2O)_4]$ (**3**), i.e., the core metric parameters are typical of the Mn_{12} family. This can be seen visually in Figure S3 in the Supporting Information, which shows the best calculated **2** vs **1** and **2** vs **3** core overlays, with the weighted root-mean-square deviations (Table S1 in the Supporting Information)[35] over the entire molecules being only 0.132 and 0.102 Å, respectively.

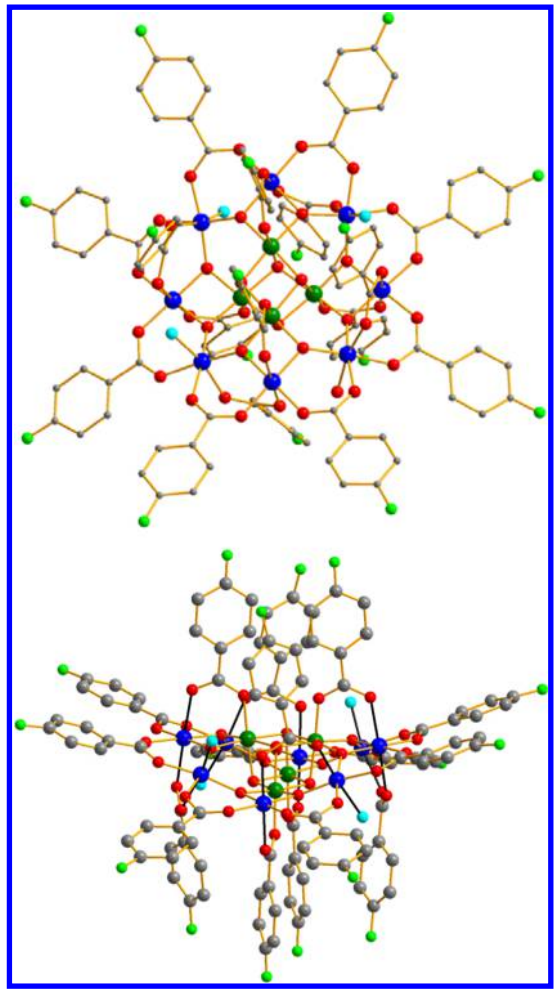

Figure 1. Structure of one disorder component of complex **2** from two near-perpendicular viewpoints. H atoms are omitted for clarity, and Mn^{III} JT axes are indicated as black bonds in the lower figure. Color code: blue, Mn^{III}; green, Mn^{IV}; red, O; sky blue, H_2O; light green, F; and gray, C.

(c) There is extensive intermolecular C−H···F hydrogen-bonding involving F atoms of one molecule and *ortho* or *meta* C−H groups of neighboring molecules. There are three types (see Figure 2): (i) Fluorines F1 on equatorial ligands hydrogen bonding with *meta*-H14 (of axial ligands bridging $Mn^{III}Mn^{IV}$ pairs; F1···C14 = 2.885(10) Å) and *ortho*-H23 (of axial ligands bridging $Mn^{III}Mn^{III}$ pairs; F1···C23 = 3.098(12) Å) (Figure 2a); (ii) Fluorines F2 on axial ligands bridging $Mn^{III}Mn^{IV}$ pairs hydrogen bonding with two equatorial *meta*-H6 on two different neighboring molecules (F2···C6 = 3.025(11) Å) (Figure 2b); and (c) Fluorines F3 on axial ligands bridging $Mn^{III}Mn^{III}$ pairs hydrogen bonding with two equatorial *ortho*-H7 of ligands on the same neighboring molecule (F3···C7 = 3.066(10) Å) (Figure 2c). Overall, each Mn_{12} hydrogen-bonds to 12 neighboring molecules (48 total hydrogen bonds, 4 per neighbor).

Magnetic Susceptibility Studies. Variable-temperature, solid-state magnetic susceptibility data were collected in a 0.1 T

DOI: 10.1021/acs.inorgchem.7b01676
Inorg. Chem. 2017, 56, 10706−10716

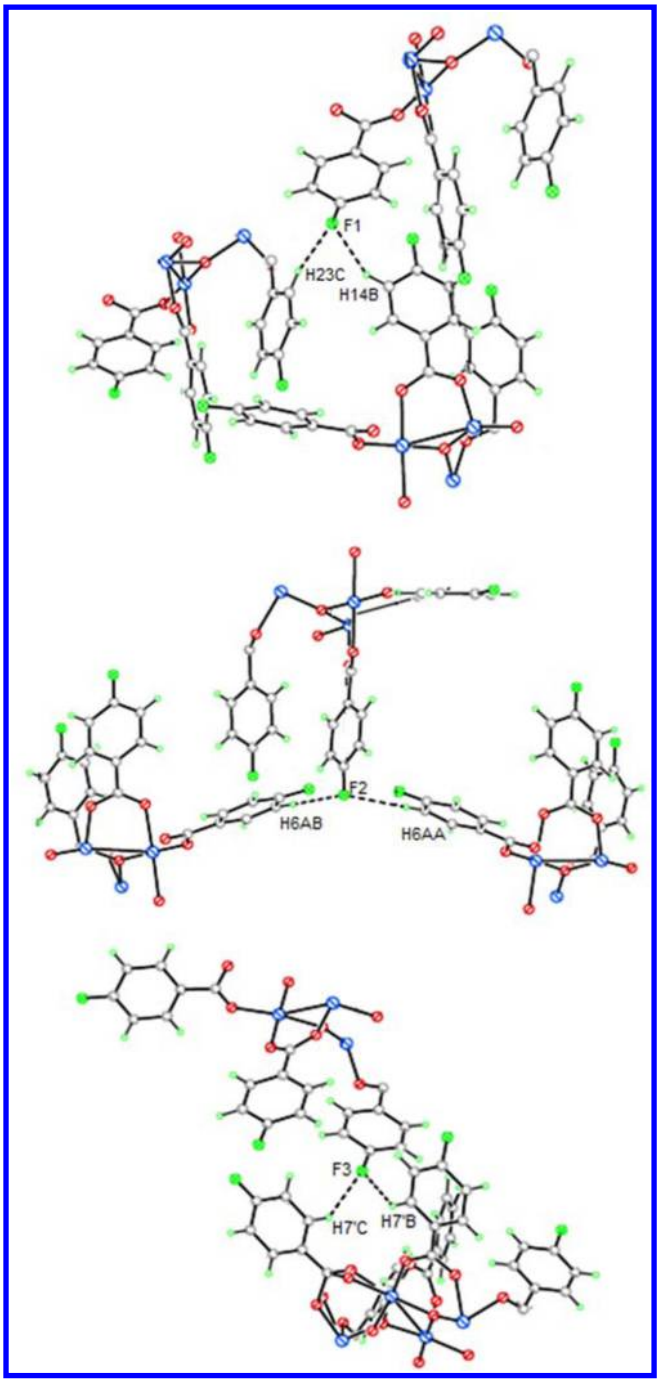

Figure 2. Three types of C−H···F hydrogen-bonds in **2**·8MeCN involving (top) F atoms F1 on equatorial ligands, and (middle and bottom) F atoms F2 and F3 on axial ligands. See the text for a fuller description. Color code: blue, Mn; red, O; solid green, F; and open green, H.

dc magnetic field in the 5.0−300 K range on (i) powdered microcrystalline "wet" samples of **2**·8MeCN (i.e., freshly taken from mother liquor, rinsed with MeCN, and dried with tissue paper), and (ii) vacuum-dried samples. All samples were restrained in eicosane to prevent torquing. After some preliminary measurements, it became clear that the data for (i) were unusual, and those for (ii) were highly dependent on the time of vacuum-drying and subsequent exposure to air. For this reason, systematic measurements were performed under different drying times and exposure to air, and the results are described below.

Magnetic Susceptibility of the Wet Sample. The $\chi_M T$ vs T plot for "wet" microcrystalline **2**·8MeCN is shown in Figure 3, where it is compared with that for **1**. The latter is

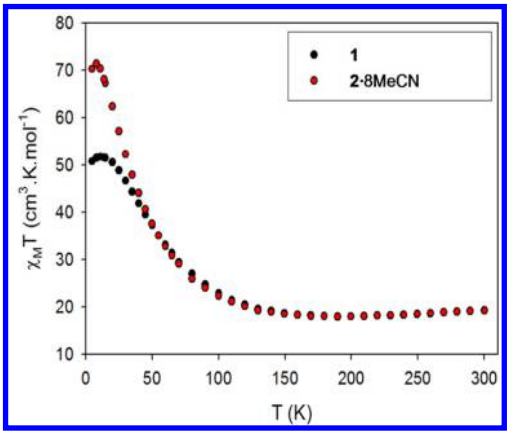

Figure 3. Plots of $\chi_M T$ vs T for **1** and **2**·8MeCN in a 0.1 T dc field.

typical for Mn_{12} clusters. The maximum of 50−55 cm^3 K mol^{-1} at low T is due to an S = 10 ground state (with g < 2.0 slightly, as expected for a $Mn^{III/IV}$ system) arising from both ferromagnetic (F) and antiferromagnetic (AF) intramolecular exchange interactions. The data for **2**·8MeCN between 60 and 300 K are identical to those for **1**, but at temperatures <60 K, they deviate and increase to a maximum of 71.4 cm^3 K mol^{-1} at 10.0 K, before showing a small decrease assignable to zero-field splitting and Zeeman effects. The origin of this high $\chi_M T$ at low T was not immediately obvious, but it was reproduced multiple times with multiple preparations (however, the crystals start losing MeCN upon removal from mother liquor and the peak appeared slightly lower at ∼68 cm^3 K mol^{-1} if it took longer than usual to get the crystals into protective eicosane). One explanation considered was that the high $\chi_M T$ was due to an S = 11 or 12 ground state ($\chi_M T$ of 66 and 78 cm^3 K mol^{-1} for g = 2.0, respectively). Since the S = 10 ground state of the Mn_{12} family arises from antiparallel alignment of 8 Mn^{III} and 4 Mn^{IV} spins, giving S = 16 − 6 = 10, an increase in S would likely require significant structural perturbation of the core. However, the near superimposable core of **2** with those of S = 10 species **1** and **3** (vide supra and Figure S3) suggested this explanation to be very unlikely.

Another possible explanation was that the high $\chi_M T$ was induced by the dc field, possibly by causing components of excited states with S > 10 to cross below the ground state, and to test this we removed the dc field. Shown in Figure 4 are the in-phase (χ'_M, as $\chi'_M T$) and out-of-phase (χ''_M) ac susceptibilities of **1** and **2**·8MeCN in a zero dc field and a 3.5 G ac field at a 1000 Hz oscillation frequency. **1** displays the expected behavior for a well-isolated S = 10 ground state, with T-independent $\chi'_M T$ above 10 K of ∼52 cm^3 K mol^{-1}. Below 10 K, $\chi'_M T$ drops and a χ''_M signal appears, as expected for the slow relaxation of an SMM. In contrast, $\chi'_M T$ for **2**·8MeCN is much larger and increases with decreasing T from 70.3 cm^3 K mol^{-1} at 15 K to a plateau maximum of 74.8 cm^3 K mol^{-1} at 8.0−9.0 K, and then decreases due to slow relaxation. The small signals in the 2−3 K range are due to FR JT isomers (vide infra). The ac data thus confirm that the high $\chi_M T$ is not due to the applied dc field. In addition, the increasing $\chi'_M T$ with decreasing T suggests the

DOI: 10.1021/acs.inorgchem.7b01676
Inorg. Chem. 2017, 56, 10706−10716

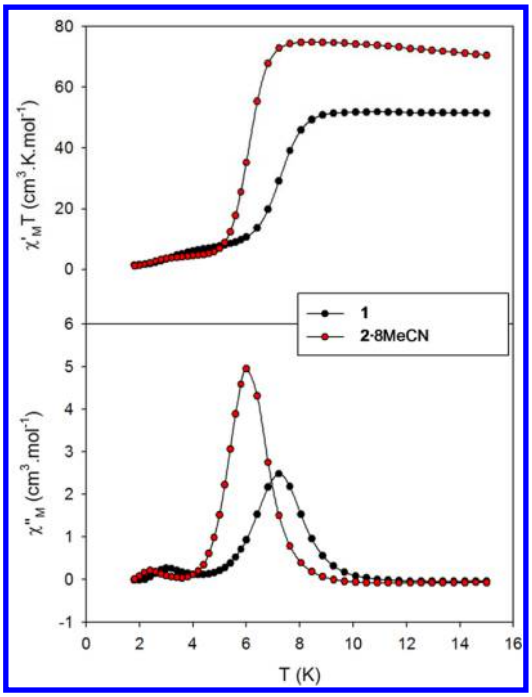

Figure 4. Plots of the in-phase (χ'_M, as $\chi'_M T$) and out-of-phase (χ''_M) ac magnetic susceptibility vs T for a wet sample of **2**·8MeCN at a 1000 Hz ac oscillation frequency.

presence of weak F interactions between neighboring Mn_{12} molecules, which would explain both the high dc $\chi_M T$ and ac $\chi'_M T$ values. An Arrhenius plot of $\ln(1/\tau)$ vs $1/T$, where τ is the relaxation time, using data collected in the 5−1500 Hz range (Figures S4 and S5 in the Supporting Information)[35] gave an effective barrier to magnetization relaxation of U_{eff} = 59.3 K and $1/\tau_0 = 3.3 \times 10^8$ s^{-1}, typical values for the Mn_{12} family with S = 10, again supporting the unusually high $\chi_M T$ and $\chi'_M T$ values not to be due to a change in ground state.

To test the hypothesis that net intermolecular **F** interactions (a relatively rare situation) are present in **2**·8MeCN, the C−H···F hydrogen bonds between Mn_{12} molecules were analyzed for their magnetic consequences. As described above and in Figure 2, there are three types involving either *ortho* or *meta* C−H units, but this minimal difference is nevertheless predicted to lead to different exchange interactions. It is known that parallel spin in Mn d_π magnetic orbitals can spread into the π-system of benzoate groups via a π-spin delocalization mechanism, leading to parallel spin in the C p_z orbitals at the *ortho* and *para* positions, in turn leading to antiparallel spin at the *ortho* and *para* H atoms through spin polarization of the C−H bond.[37] Since F has a π-symmetry p_z orbital, parallel spin will also π-delocalize directly from the *ortho* C p_z into the F p_z (Figure 5). In contrast, parallel spin in the *ortho* and *para* C p_z orbitals will lead to antiparallel spin in the *meta* C p_z and thus parallel spin in the *meta* H atom from spin polarization. We can thus predict the following exchange interactions for the two types of C−H···F H-bonds:

(A) For those involving *ortho* C−H groups, net overlap between the F p_z orbital and the C−H group (the C−F···C angles are all <180°) gives a local AF interaction, but since the H spin is opposite to that in the Mn_{12} core, this gives a net F interaction between the two Mn_{12} neighbors (Figure 5, top).

(B) For the *meta* C−H groups, the same AF C−H···F overlap occurs, but since the H spin is the same as on the Mn_{12} core, there is now a net AF interaction between the Mn_{12} neighbors (Figure 5, bottom). Both types of interaction should be very weak, but those involving *ortho* C−H groups are likely to be slighter stronger, given the greater spin delocalized onto the *ortho* positions. Although difficult to predict a priori, it is reasonable that the net sum of the many F and AF contributions to the overall intermolecular interaction should be F and significant enough to have a noticeable effect, giving the unusually high dc $\chi_M T$ and ac $\chi'_M T$ values for **2**·8MeCN at low T.

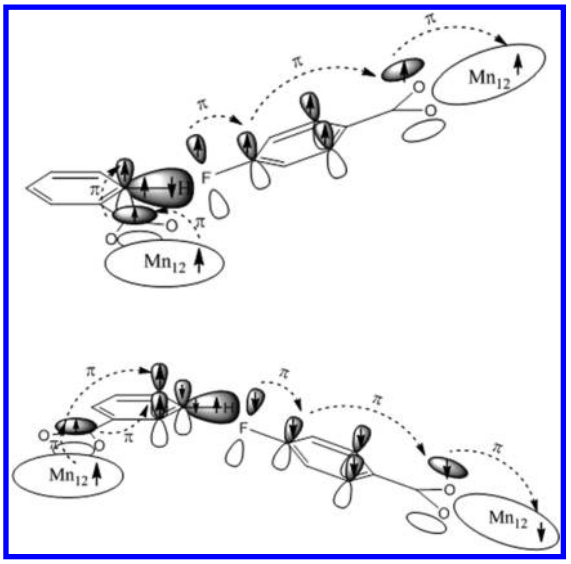

Figure 5. Two types of hydrogen bonding in **2**·8MeCN. The top panel shows F···HC(*ortho*) contacts, leading to net F interactions between neighboring Mn_{12} molecules; and the bottom panel shows F···HC(*meta*) contacts leading to net AF interactions.

An estimate of the magnitude of the net intermolecular F interaction was obtained from the dc $\chi_M T$ vs T data for **2**·8MeCN and related **3** (Figure 6) using the molecular field approach.[38,39] The plot for **3** is essentially superimposable with that of **1** and was assumed to involve insignificant intermolecular interactions, consistent with its structure.[40] The value of zJ_F/k was then adjusted to simulate the data for **2**·8MeCN, where z is the number of nearest-neighbor molecules, J_F is the net intermolecular exchange parameter, and k is the Bohr magneton. The best simulation (solid line in

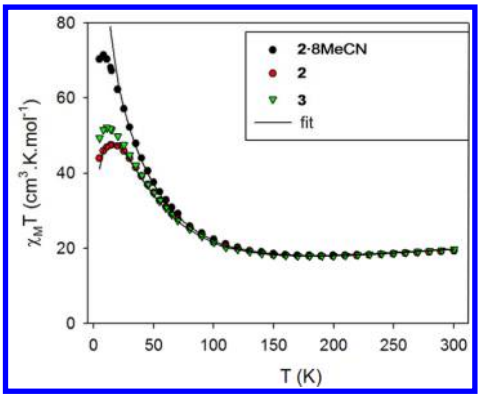

Figure 6. Simulation of the dc $\chi_M T$ vs T data for **2**·8MeCN and vacuum-dried **2** using the $\chi_M T$ vs T data for **3** and a mean-field approach. See the text for the simulation parameters.

DOI: 10.1021/acs.inorgchem.7b01676
Inorg. Chem. 2017, 56, 10706−10716

Figure 6) was obtained with zJ_F/k = +0.070(10) K, i.e., F and extremely weak, as expected. However, even though the exchange parameter is very small, note that the exchange energy ($-2JS_iS_j$) will be significant, because of the large S = 10, leading to markedly different $\chi_M T$ data for **2**·8MeCN vs **3**.

Vacuum Drying of 2·8MeCN. A large batch of **2**·8MeCN crystals was prepared and samples were vacuum-dried for different times (including zero drying) before magnetic study. The dc $\chi_M T$ vs T plots are shown in Figure 7. Drying causes a large decrease in the $\chi_M T$ at low T, reaching a peak value of 49.9 cm^3 K mol^{-1} after 1 h. A second hour of drying causes only a small further decrease, to 47.5 cm^3 K mol^{-1}, indicating changes to be complete, and elemental analysis of this material analyzed as solvent-free **2** (see the Experimental Section). $\chi_M T$ for **2** is slightly lower than the 50−55 cm^3 K mol^{-1} range expected for an S = 10 Mn_{12} molecule, suggesting that vacuum drying causes a change from net intermolecular F to net AF interactions. The ac data collected on the same set of samples supported this conclusion (Figure 8): below 15 K, the rising slope of the $\chi'_M T$ of wet sample becomes essentially T-independent at ∼50 cm^3 K mol^{-1} after drying for 1 h, and then decreases slightly further and exhibits a very slight negative slope after drying for 2 h, supporting very weak net AF interactions. We thus conclude that the loss of lattice MeCN molecules somehow causes a switching of the net intermolecular interactions from weakly F to very weakly AF. There is also an interesting variation in the magnitude of the FR signal in the 2−3 K range during the vacuum drying (vide infra).

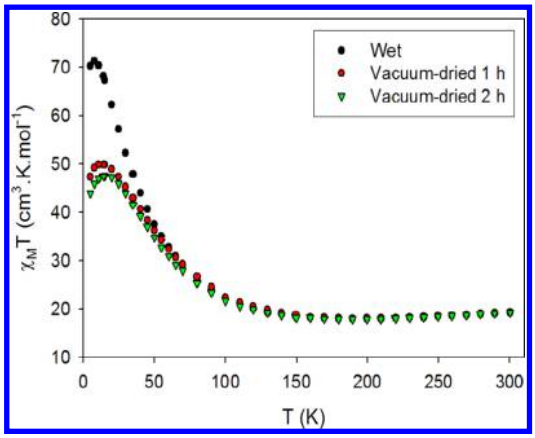

Figure 7. Plots of dc $\chi_M T$ vs T data for **2**·8MeCN after 0, 1, and 2 h of vacuum drying.

The magnitude of the net AF intermolecular interactions was again estimated using the molecular field approach and the dc $\chi_M T$ vs T data for vacuum-dried **2** and complex **3**. An excellent simulation was obtained (Figure 6) with zJ_{AF}/k = −0.015(5) K, i.e., AF and significantly weaker than J_F in **2**·8MeCN, consistent with the observed changes in $\chi_M T$ between **2**·8MeCN and **2**. The Arrhenius plot of $\ln(1/\tau)$ vs $1/T$ for **2** (Figure S5 in the Supporting Information)[35] gave U_{eff} = 60.6 K and $1/\tau_0 = 3.3 \times 10^8$ s^{-1}, essentially identical with those for **2**·8MeCN.

Exposure of Dried 2 to Air. After 2 h of drying, samples of **2** were exposed to air and $\chi_M T$ recorded after various exposure times, with each sample being weighed and embedded into eicosane. The obtained plots (Figure 9) show the reverse behavior to that seen on drying, i.e., $\chi_M T$ at low T now increases with time, the peak value being 47.5, 50.9, 53.9, 59.0, and 61.2 cm^3 K mol^{-1} for 0, 1, 4, 16, and 32 h exposure, respectively, after which time it no longer changed. The dried sample was absorbing moisture, as confirmed by elemental analysis of material exposed for >32 h as **2**·3H_2O. Clearly, whatever was occurring on loss of the MeCN molecules during drying could be reversed on absorption of water, at least partially because the $\chi_M T$ does not return to its original value for **2**·8MeCN. Nevertheless, $\chi_M T$ = 61.2 cm^3 K mol^{-1} is still larger than the 55 cm^3 K mol^{-1} for S = 10 with g = 2, indicating that the sample had reverted from net AF interactions in **2** back to net F in **2**·3H_2O. Again, the ac $\chi'_M T$ data (Figure 10) showed the same behavior as the dc $\chi_M T$, and, in addition, $\chi'_M T$ for the 32 h sample increased with decreasing T, as expected for net F interactions. Now, there were dramatic changes in the

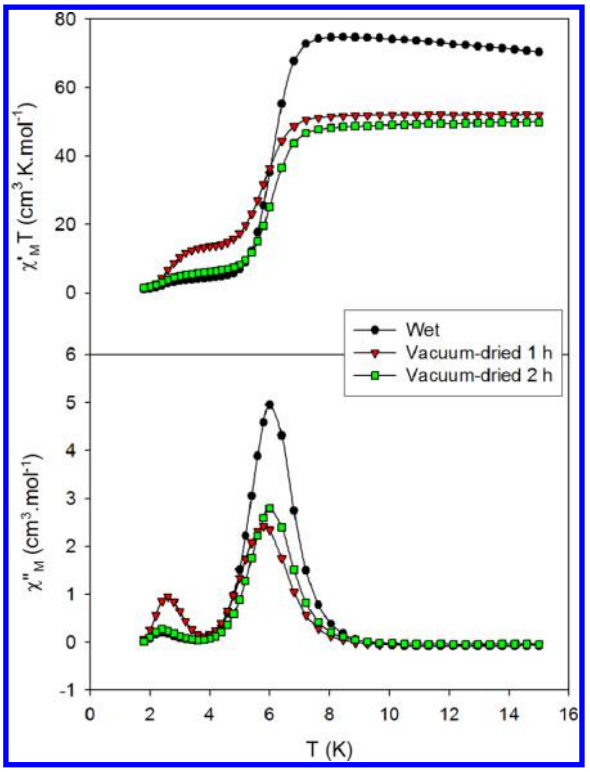

Figure 8. Plots of ac susceptibility data for **2**·8MeCN after 0, 1, and 2 h of vacuum drying: (top) in-phase $\chi'_M T$ vs T and (bottom) out-of-phase χ''_M vs T. The samples are the same as those used in Figure 7. The ac oscillation frequency was 1000 Hz.

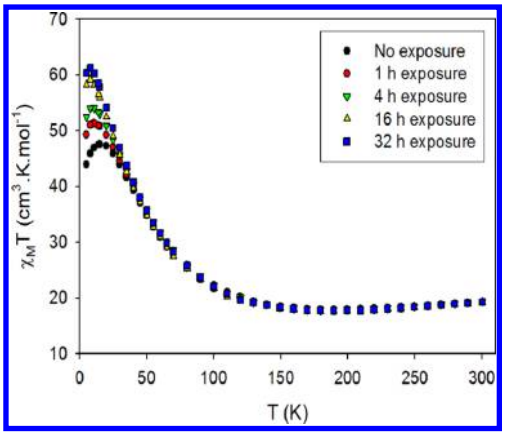

Figure 9. Plots of dc $\chi_M T$ vs T data for vacuum-dried **2** after the indicated times of exposure to air. There was no further change after 32 h.

DOI: 10.1021/acs.inorgchem.7b01676
Inorg. Chem. 2017, 56, 10706−10716

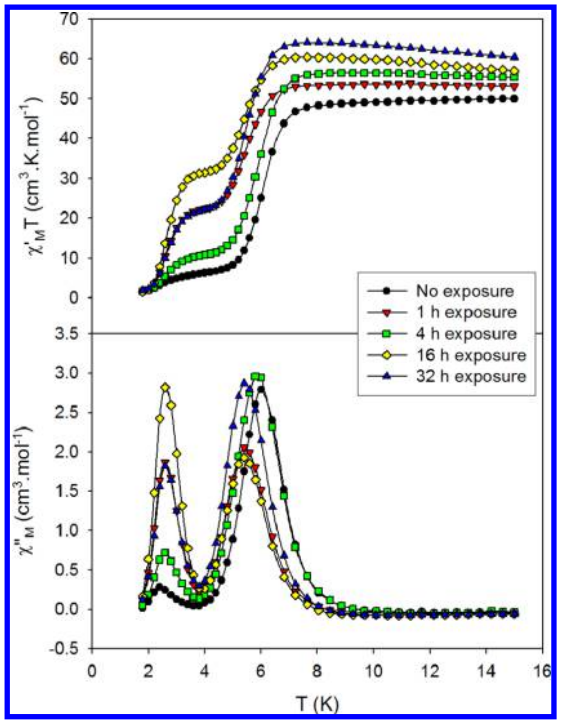

Figure 10. Plots of ac susceptibility data for vacuum-dried **2** after the indicated times of exposure to air: (top) in-phase $\chi'_M T$ vs T and (bottom) out-of-phase χ''_M vs T. The samples are the same as those used in Figure 9. The ac oscillation frequency was 1000 Hz.

magnitude of the FR signal in the 2−3 K range (vide infra). The Arrhenius plot of $\ln(1/\tau)$ vs $1/T$ for **2**·3H$_2$O (Figure S5 in the Supporting Information)[35] gave U_{eff} = 59.6 K and $1/\tau_0 = 3.3 \times 10^8$ s^{-1}, essentially identical to those for **2**·8MeCN and **2**.

Unit-Cell Dimensions. Further insights were obtained when it was realized that the drying of **2**·8MeCN, and subsequent exposure to air, only partially degraded the crystals and they still diffracted adequately for unit-cell dimensions to be obtained (Table 2). The cell volume decreases by ∼17%

Table 2. Unit-Cell Parameters for Complexes 2·8MeCN, 2, and 2·3H$_2$O

	Value			
parameter	**2**·8MeCN[a]	**2**[b,c]	**2**·3H$_2$O[d,e]	**2**·3H$_2$O[f,g]
a (Å)	17.4099(12)	17.01(4)	17.4(1)	17.3(1)
b (Å)	17.4099(12)	17.01(4)	17.4(1)	17.3(1)
c (Å)	23.8737(17)	20.73(5)	21.6(1)	21.1(1)
$\alpha = \beta = \gamma$ (deg)	90	90	90	90
V (Å^3)	7236.2(11)	5994(25)	6500(80)	6300(80)
cryst syst	tetragonal I	tetragonal P	tetragonal P	tetragonal P

[a]As isolated from the mother liquor. [b]Vacuum-dried for 2 h. [c]Using 162 reflections. [d]Vacuum-dried for 2 h and then exposed to air for 32 h. [e]Using 77 reflections. [f]As isolated, exposed to air for 10 days. [g]Using 507 reflections.

upon drying to **2**, from 7236 Å^3 to 5994 Å^3, and expands to 6500 Å^3 upon hydration. This is consistent with the relative solvent content in the three materials. Interestingly, the volume changes are primarily due to changes to the c-axis, which decreases ∼13% from 23.9 Å to 20.7 Å upon drying and then back to 21.6 Å upon hydration. In contrast, the a- and b-axes undergo minimal change. The structure of **2**·8MeCN thus collapses dramatically along the c-axis upon drying, which is a process that is only partially reversible. This process is summarized in Figure 11; note that the c-axis is parallel to the z-axes (easy axes) of the Mn$_{12}$ molecules.

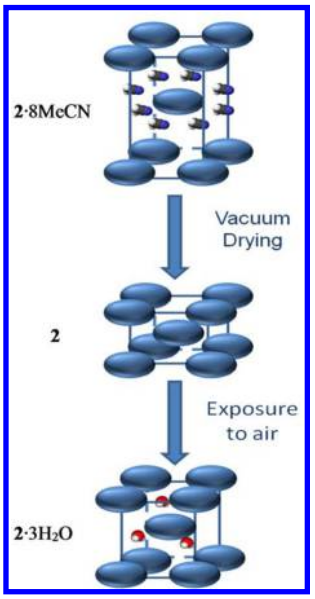

Figure 11. Diagrammatic representation of the changes in unit-cell parameters of **2**·8MeCN induced by drying under vacuum and subsequent exposure to air. Only the eight MeCN and three H$_2$O molecules for the central Mn$_{12}$ are included, placed at arbitrary positions. The crystal c- and molecular z-axes are both vertical.

Exposure of 2·8MeCN to air. The ready loss of MeCN from **2**·8MeCN crystals under vacuum and even at atmospheric pressure upon removal from mother liquor, and the ready absorption of water by vacuum drying **2**, suggested a low and high affinity for MeCN and H$_2$O, respectively.

Thus, instead of performing this solvent change sequentially, we also allowed this to occur contemporaneously by taking **2**·8MeCN crystals from mother liquor, dabbing them dry with tissue, and maintaining them at ambient temperature and pressure for 10 days. The resulting crystals analyzed as **2**·3H$_2$O and gave unit-cell dimensions (Table 2) and dc $\chi_M T$ and ac $\chi'_M T$ and χ''_M plots vs T (Figure S6 in the Supporting Information) identical (within uncertainties) with those for **2**·3H$_2$O prepared sequentially by vacuum-drying and exposure to air. Thus, exposure to air of the larger unit cell of **2**·8MeCN does not allow more than three water molecules to be absorbed. For completeness, we also submerged vacuum-dried **2** for 3 days in dried liquid MeCN in a sealed vessel to see if we could force reabsorption of MeCN. However, the subsequent $\chi_M T$ vs T plot (Figure 12) was identical to that of **2**·3H$_2$O, indicating that the crystals instead have scavenged water, confirmed by the elemental analysis showing no MeCN (only trace N), but the crystals had degraded too much for a unit-cell determination. These results are all consistent with the strong O−H···O hydrogen bonds expected between water and the carboxylate ligands of **2**.

Jahn−Teller Isomers. As stated above, the Mn^{III} JT axis in Mn$_{12}$ SMMs can be found abnormally oriented toward a μ_3−O^{2-} ion.[2] Such so-called JT isomers have a significantly smaller U_{eff}, are faster-relaxing (FR) than the normal slower-relaxing (SR) Mn$_{12}$, and their χ''_M signals are thus typically in the 2−4 K

DOI: 10.1021/acs.inorgchem.7b01676
Inorg. Chem. 2017, 56, 10706−10716

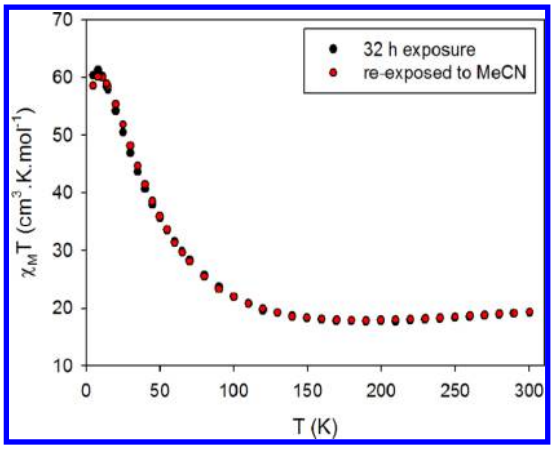

Figure 12. Comparison of the dc $\chi_M T$ vs T data for **2**·3H_2O (from vacuum-dried **2** exposed to air for 32 h, denoted by solid black circles), and vacuum-dried **2** submerged in liquid MeCN for 3 days (denoted by solid red circles).

range (for ac frequencies of ≤1500 Hz) rather than the 6−8 K for the SR Mn_{12}.[36,41] Often, FR and SR isomers occur together in the same sample, with the latter usually being the majority component, but occasionally samples are found to consist of only FR isomers. The $[Mn_{12}O_{12}(O_2CR)_{16}(H_2O)_4]\cdot CH_2Cl_2\cdot$solv (R = $CH_2{}^tBu$; solv = $MeNO_2$ or MeCN) is a particularly instructive pair, since the two solvates crystallize in the same space group with approximately identical cell parameters and with the $CH_2Cl_2/MeNO_2$ or CH_2Cl_2/MeCN molecules in essentially identical positions—and yet they are 100% FR and SR, respectively.[36b] This major difference in magnetic properties arising from such a tiny environmental difference points to a very small energy difference between the two JT isomers, and, indeed, the FR form converts to the SR form upon allowing the crystal to slowly lose solvent, indicating that the latter is the thermodynamically preferred form. Furthermore, crystals of several Mn_{12} complexes consisting of 100% SR isomer have been seen to convert to a mixture of SR and FR forms upon vacuum drying, further supporting a small energy difference between them.[42]

These previous observations allow us to rationalize the ac data for the various solvate forms of **2** in the present work. **2**·8MeCN is mainly SR, as is **1**, with a weak (<5%) peak that is due to the FR form (see Figure 4). However, the amount of the latter changes significantly during vacuum drying to **2** and subsequent hydration to **2**·3H_2O, but not in a monotonic way. Vacuum drying of **2**·8MeCN for 1 and 2 h (Figure 8) causes an increase and then a decrease, respectively, in the FR amount. Similarly, exposure of dried **2** to air causes multiple increases and decreases in the FR amount. Given the recognized small energy difference between FR and SR forms, we can qualitatively rationalize this as being due to small environmental changes at each Mn_{12} molecule as the solvent content of the solid changes, and the crystal lattice adjusts slightly, imposing some strain on the Mn_{12} molecules and causing the JT isomerization. However, the strain obviously varies as the total solvent content changes during the drying or hydration, giving multiple stages with different FR:SR ratios. An Arrhenius plot (Figure S7 in the Supporting Information) constructed for the low-T FR species gave U_{eff} = 36.5 K and $1/\tau_0 = 5.2 \times 10^9$ s^{-1}. These are typical values for the FR Mn_{12} JT isomers; for example, those for FR $[Mn_{12}O_{12}(O_2CCH_2{}^tBu)_{16}(H_2O)_4]\cdot CH_2Cl_2\cdot MeNO_2$ are U_{eff} = 42 K and $1/\tau_0 = 4.5 \times 10^9$ s^{-1}.[36b]

Magnetization Hysteresis Studies. Since Mn_{12} SMMs exhibit hysteresis loops with well-resolved quantum tunneling of magnetization (QTM) steps,[2] intermolecular interactions could lead to the observation of exchange-biased QTM, i.e., neighboring molecules acting as bias fields that shift the QTM step positions. Therefore, magnetization hysteresis studies were performed on an aligned single crystal of **2**·8MeCN, using a micro-SQUID apparatus with the applied field along the crystal c-axis (Mn_{12} easy (z)-axis).

Figure 13 shows the resulting hysteresis loops at 0.140 T/s in the 3.2−4.6 K range (Figure 13a), and at 3.6 K in the 0.002−

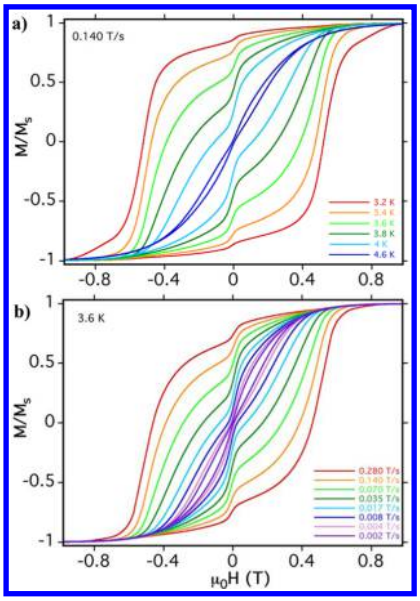

Figure 13. Magnetization (M) vs dc field (H) scans for a single crystal of **2**·8MeCN, showing (a) the temperature dependence of the hysteresis loops at 0.140 T/s and (b) the scan-rate dependence at 3.6 K. The magnetization is normalized to its saturation value, M_s.

0.280 T/s scan rate (Figure 13b). Only at temperatures >3 K is the QTM step at zero field clearly observed; a fuller version of Figure 13a spanning the 1.3−4.6 K range is given in Figure S8 in the Supporting Information. The coercivity increases with decreasing T and increasing scan rate, as expected for an SMM. The QTM steps are not as sharp as they typically are in Mn_{12} SMMs, which is assigned to broadening from the intermolecular interactions and the extensive ligand disorder, giving a distribution of molecular environments and local site symmetries. It is not readily apparent from Figure 13 whether the first step is slightly shifted from zero field, but the first derivative of the hysteresis loops (Figure 14a) confirms a very small exchange bias field of H_{ex} = −0.012 T, indicating the presence of a very weak net AF intermolecular interaction.

On first thought, this appears to be in conflict with the dc and ac studies concluding a net F intermolecular interaction. However, this is not the case, and the two conclusions are compatible in **2**·8MeCN for the following reason: The single-crystal micro-SQUID study applies a field along the easy-axis (molecular z-direction), and molecules can exhibit QTM when m_S states of the S = 10 spin manifold on one side of the anisotropy barrier are degenerate with m_S states on the other side.[43] This occurs at zero field for the $\pm m_S$ pairs of a molecule not exchange-coupled to neighbors; thus, the first step is at zero field. When there are intermolecular interactions, the longitudinal (J_z) components of these interactions will provide

DOI: 10.1021/acs.inorgchem.7b01676
Inorg. Chem. 2017, 56, 10706−10716

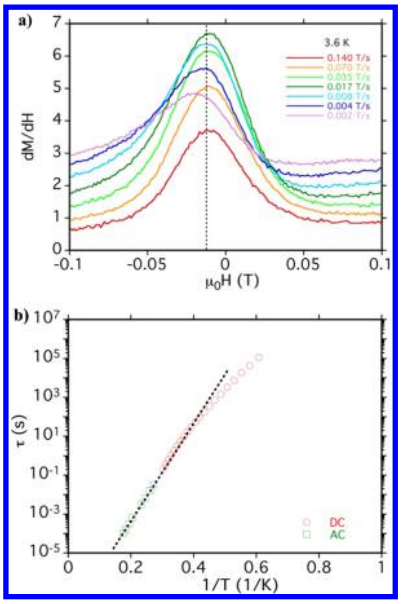

Figure 14. (a) Data for a single crystal of **2**·8MeCN from Figure 13b plotted as dM/dH to better identify the position of the QTM step near zero field. (b) Arrhenius plot constructed from dc magnetization decay versus time data and ac in-phase $\chi'_M T$ vs T data. The dashed line is a fit of the higher-T to obtain U_{eff} and τ_0. See the text for the fit parameters.

a bias field from neighboring molecules that adds to the applied field, shifting the position of the zero-field QTM step slightly away from zero.

A transverse bias from transverse components (J_x, J_y) will influence the tunnel splitting and also give a sloping background to the hysteresis loops, but will not contribute in the z-direction and will not therefore affect the step shift. The bottom line is that the hysteresis loop is affected only by components of intermolecular interactions along the easy-axis (z-axis) of the molecules (crystal c-axis), because that is the applied field direction, and the observed $H_{ex} = -0.012$ T shows that the net interaction in this direction is AF. The exchange bias gives a calculated net value of $J_z = -0.70 \times 10^{-3}$ cm^{-1} = −1.0 mK, using eq 2 and the knowledge from previous work on Mn_{12} SMMs that the dominating relaxation pathway at T = 3.6 K involves mostly the m_S = 4 energy level.[44]

$$H_{ex} = \frac{2J_z m_S}{g\mu_B} \quad (2)$$

Given the large number and different types of intermolecular exchange interactions in **2**·8MeCN, it is reasonable that there would be such a weak net AF interaction along the z-axis, even though the overall interaction between Mn_{12} molecules is F.

dc magnetization decay versus time data were collected, as described elsewhere,[45] on the same crystal of **2**·8MeCN (Figure S9 in the Supporting Information) and used to obtain additional ln($1/\tau$) vs $1/T$ data to supplement those from ac data; the resulting Arrhenius plot (Figure 14b) over a greater T range gave more-reliable values of U_{eff} = 56.4 K and $1/\tau_0 = 1.4 \times 10^8$ s^{-1}, compared with U_{eff} = 59.3 K, and $1/\tau_0 = 3.3 \times 10^8$ s^{-1} from the ac data alone.

CONCLUSIONS

Even after all the years since its initial report, the Mn_{12} family of SMMs continues to surprise. The new complex, **2**·8MeCN, is the first example of a three-dimensional (3-D) ferromagnetic network of Mn_{12} clusters, arising from a combination of ferromagnetic (F) and antiferromagnetic (AF) interactions mediated by the many intermolecular C−H···F hydrogen bonds in the crystal. We rationalize this mixture of F and AF as arising from the *ortho*- vs *meta*-positions of the C−H bonds involved, but also emphasize the importance of the π-symmetry orbital on the p-F atom, which allows direct π-spin delocalization onto the F and, thus, intermolecular exchange interactions of significant magnitude. The loss of MeCN molecules upon drying induces a collapse of the lattice and a switch to a net AF network. Since the MeCN molecules are not involved in the intermolecular hydrogen bonds, we suspect that (i) the latter are not greatly disrupted, and thus (ii) the switch to an AF network is perhaps not due to a loss of intermolecular F contacts but an increase in AF ones, e.g., by better overlap of π-systems of neighboring molecules. We did collect data on a crystal of vacuum-dried **2** in an attempt to gain better insights into this, but the resulting structure was too poor to provide useful information.

Thus, the switch back to a F network in **2**·3H_2O probably is simply due to the re-expansion of the unit cell as it absorbs water molecules. We refrain from calling this a reversible switch, since we are not reinserting MeCN, and we are also unable to remove the water molecules to cycle the changes. For the same reason, this is not a magnetic sponge, which is a description best reserved for multiple cycles of reversible solvent loss and gain, as well-established, for example, in MOF chemistry.[46,47]

The formation of FR JT isomer upon drying is not unprecedented, but what was unexpected was the oscillation of its amount during the hydration process. It invokes a picture of varying strain at different points inside the crystals, and on the Mn_{12} molecules, as water progressively diffuses in and the unit cells expand. The final FR:SR ratio after >32 h exposure was essentially reproducible, including for the exposure of **2**·8MeCN to air for 10 days (Figure S6c in the Supporting Information); we did wonder whether, at much greater exposure times, the crystals would "anneal" to give just the SR isomer, but exposing vacuum-dried **2** to air for >7 days gave the same FR:SR ratio. We assign this to the nonreversible degradation of the crystallinity. Finally, we note that the intrinsic magnetic properties of the SR Mn_{12} molecules do not change during the various solvent loss and gain, as judged by the resulting U_{eff} values, other than the fact that some have switched to the FR form, of course. This is in contrast to some results in the literature that have concluded that the desolvation/solvation steps lead to changes in the magnetic properties due to intramolecular structural changes to the magnetic molecules.[20] The Mn/O core is obviously overall very robust, but nevertheless easily susceptible to JT isomerization, again reflecting the very small energy difference involved in the latter.

ASSOCIATED CONTENT

Supporting Information

The Supporting Information is available free of charge on the ACS Publications website at DOI: 10.1021/acs.inorgchem.7b01676.

Crystallographic details for **2**·8MeCN in CIF format, structural figures, bond valence sums, bond distances and angles, magnetic data (PDF)

DOI: 10.1021/acs.inorgchem.7b01676
Inorg. Chem. 2017, 56, 10706−10716

Accession Codes

CCDC 1559496 contains the supplementary crystallographic data for this paper. These data can be obtained free of charge via www.ccdc.cam.ac.uk/data_request/cif, or by emailing data_request@ccdc.cam.ac.uk, or by contacting The Cambridge Crystallographic Data Centre, 12 Union Road, Cambridge CB2 1EZ, UK; fax: +44 1223 336033.

AUTHOR INFORMATION

Corresponding Author

*E-mail: christou@chem.ufl.edu.

ORCID

George Christou: 0000-0001-5923-5523

Present Address

§Intel Corporation, Hillsboro, OR.

Notes

The authors declare no competing financial interest.

ACKNOWLEDGMENTS

This work was supported by the USA National Science Foundation (GC: CHE-1565664). W.W. acknowledges support from the EU by the FP7 FET-Proactive project MoQuaS (No. 610449) and the Agence Nationale de la Recherche project MolQuSpin (No. ANR-13-BS10). We thank Rodolphe Clérac for the molecular field fits.

REFERENCES

(1) Lis, T. Preparation, structure, and magnetic properties of a dodecanuclear mixed-valence manganese carboxylate. *Acta Crystallogr., Sect. B: Struct. Crystallogr. Cryst. Chem.* **1980**, *36*, 2042−2046.

(2) Bagai, R.; Christou, G. The *Drosophila* of single-molecule magnetism: $[Mn_{12}O_{12}(O_2CR)_{16}(H_2O)_4]$. *Chem. Soc. Rev.* **2009**, *38*, 1011−1026.

(3) Aromi, G.; Brechin, E. K. Synthesis of 3d metallic single-molecule magnets. *Struct. Bonding (Berlin)* **2006**, *122*, 1−68.

(4) Gatteschi, D.; Sessoli, R.; Villain, J. *Molecular Nanomagnets*; Oxford University Press: Oxford, U.K., 2006.

(5) Woodruff, D. N.; Winpenny, R. E.; Layfield, R. A. Lanthanide single-molecule magnets. *Chem. Rev.* **2013**, *113*, 5110−5148.

(6) Rinehart, J. D.; Long, J. R. Slow magnetic relaxation in a trigonal prismatic uranium(III) Complex. *J. Am. Chem. Soc.* **2009**, *131*, 12558−12559.

(7) (a) Pereira, L. C. J.; Camp, C.; Coutinho, J. T.; Chatelain, L.; Maldivi, P.; Almeida, M.; Mazzanti, M. Single-molecule magnet behavior in mononuclear homoleptic tetrahedral uranium(III) Complexes. *Inorg. Chem.* **2014**, *53*, 11809−11811. (b) Moro, F.; Mills, D. P.; Liddle, S. T.; van Slageren, J. The inherent single-molecule magnet character of trivalent uranium. *Angew. Chem., Int. Ed.* **2013**, *52*, 3430−3433.

(8) Craig, G. A.; Murrie, M. 3d single-ion magnets. *Chem. Soc. Rev.* **2015**, *44*, 2135−2147.

(9) Friedman, J. R.; Sarachik, M. P.; Tejada, J.; Ziolo, R. Macroscopic measurement of resonant magnetization tunneling in high-spin molecules. *Phys. Rev. Lett.* **1996**, *76*, 3830−3833.

(10) Luis, F.; Bartolomé, J.; Fernández, J. F.; Tejada, J.; Hernández, J. M.; Zhang, X. X.; Ziolo, R. Thermally activated and field-tuned tunneling in Mn_{12}Ac studied by ac magnetic susceptibility. *Phys. Rev. B: Condens. Matter Mater. Phys.* **1997**, *55*, 11448−11456.

(11) McHugh, S.; Sarachik, M. P. Magnetic avalanches in molecular nanomagnets. *Mod. Phys. Lett. B* **2011**, *25*, 1795−1807.

(12) Thuijs, A. E; Christou, G.; Abboud, K. A. $[Mn_{12}O_{12}(O_2CMe)_{12}(NO_3)_4(H_2O)_4]$: Facile synthesis of a new type of Mn_{12} complex. *Acta Crystallogr., Sect. C: Struct. Chem.* **2015**, *71*, 185−187.

(13) Thuijs, A. E; Clerac, R.; Wernsdorfer, W.; Abboud, K. A.; Christou, G. Manuscript in preparation.

(14) Wernsdorfer, W.; Aliaga-Alcalde, N.; Hendrickson, D. N.; Christou, G. Exchange-biased Quantum Tunneling in a Supramolecular Dimer of Single-Molecule Magnets. *Nature* **2002**, *416*, 406−409.

(15) (a) Tiron, R.; Wernsdorfer, W.; Aliaga-Alcalde, N.; Christou, G. Quantum tunneling in a three-dimensional network of exchange-coupled single-molecule magnets. *Phys. Rev. B: Condens. Matter Mater. Phys.* **2003**, *68*, 140407. (b) Yang, E.-C.; Wernsdorfer, W.; Hill, S.; Edwards, R. S.; Nakano, M.; Maccagnano, S.; Zakharov, L. N.; Rheingold, A. L.; Christou, G.; Hendrickson, D. N. Exchange bias in Ni_4 single-molecule magnets. *Polyhedron* **2003**, *22*, 1727−1733.

(16) Das, A.; Gieb, K.; Krupskaya, Y.; Demeshko, S.; Dechert, S.; Klingeler, R.; Kataev, V.; Buchner, B.; Muller, P.; Meyer, F. A New Family of 1D Exchange Biased Heterometal Single-Molecule Magnets: Observation of Pronounced Quantum Tunneling Steps in the Hysteresis Loops of Quasi-Linear $\{Mn_2Ni_3\}$ Clusters. *J. Am. Chem. Soc.* **2011**, *133*, 3433−3443.

(17) Inglis, R.; Jones, L. F.; Mason, K.; Collins, A.; Moggach, S. A.; Parsons, S.; Perlepes, S. P.; Wernsdorfer, W.; Brechin, E. K. Ground spin state changes and 3 d networks of exchange coupled $[Mn^{III}_3]$ single-molecule magnets. *Chem.—Eur. J.* **2008**, *14*, 9117−9121.

(18) Boskovic, C.; Bircher, R.; Tregenna-Piggott, P. L. W.; Güdel, H. U.; Paulsen, C.; Wernsdorfer, W.; Barra, A.-L.; Khatsko, E.; Neels, A.; Stoeckli-Evans, H. J. *J. Am. Chem. Soc.* **2003**, *125*, 14046−14058.

(19) Bagai, R.; Wernsdorfer, W.; Abboud, K. A.; Christou, G. Exchange-biased dimers of single-molecule magnets in OFF and ON states. *J. Am. Chem. Soc.* **2007**, *129*, 12918−12919.

(20) Pinkowicz, D.; Southerland, H. I.; Avendaño, C.; Prosvirin, A.; Sanders, C.; Wernsdorfer, W.; Pedersen, K. S.; Dreiser, J.; Clérac, R.; Nehrkorn, J.; Simeoni, G. G.; Schnegg, A.; Holldack, K.; Dunbar, K. R. Cyanide Single-Molecule Magnets Exhibiting Solvent Dependent Reversible "On" and "Off" Exchange Bias Behavior. *J. Am. Chem. Soc.* **2015**, *137*, 14406−14422.

(21) (a) Nguyen, T. N.; Wernsdorfer, W.; Abboud, K. A.; Christou, G. A Supramolecular Aggregate of Four Exchange-Biased Single-Molecule Magnets. *J. Am. Chem. Soc.* **2011**, *133*, 20688−20691. (b) Nguyen, T. N.; Wernsdorfer, W.; Shiddiq, M.; Abboud, K. A.; Hill, S.; Christou, G. Supramolecular Aggregates of Single-Molecule Magnets: Exchange-biased Quantum Tunneling of Magnetization in a Rectangular $[Mn_3]_4$ Tetramer. *Chem. Sci.* **2016**, *7*, 1156−1173.

(22) Habib, F.; Lin, P.-H.; Long, J.; Korobkov, I.; Wernsdorfer, W.; Murugesu, M. The use of magnetic dilution to elucidate the slow magnetic relaxation effects of a Dy_2 single-molecule magnet. *J. Am. Chem. Soc.* **2011**, *133*, 8830−8833.

(23) Miyasaka, H.; Yamashita, M. A look at molecular nanosized magnets from the aspect of inter-molecular interactions. *Dalton Trans.* **2007**, 399−406.

(24) Mathonière, C.; Lin, H.-J.; Siretanu, D.; Clèrac, R.; Smith, J. M. Photoinduced single-molecule magnet properties in a four-coordinate iron(II) spin crossover complex. *J. Am. Chem. Soc.* **2013**, *135*, 19083−19086.

(25) Pinkowicz, D.; Ren, M.; Zheng, L.-M.; Sato, S.; Hasegawa, M.; Morimoto, M.; Irie, M.; Breedlove, B. K.; Cosquer, G.; Katoh, K.; Yamashita, M. Control of the single-molecule magnet behavior of lanthanide-diarylethene photochromic assemblies by irradiation with light. *Chem.—Eur. J.* **2014**, *20*, 12502−12513.

(26) Shiga, T.; Miyasaka, H.; Yamashita, M.; Morimoto, M.; Irie, M. Copper(II)-terbium(III) single-molecule magnets linked by photochromic ligands. *Dalton Trans.* **2011**, *40*, 2275−2282.

(27) Ren, M.; Pinkowicz, D.; Yoon, M.; Kim, K.; Zheng, L.-M.; Breedlove, B. K.; Yamashita, M. Dy(III) single-ion magnet showing extreme sensitivity to (de)hydration. *Inorg. Chem.* **2013**, *52*, 8342−8348.

(28) Norel, L.; Feng, M.; Bernot, K.; Roisnel, T.; Guizouarn, T.; Costuas, K.; Rigaut, S. Redox modulation of magnetic slow relaxation in a 4f-based single-molecule magnet with a 4d carbon-rich ligand. *Inorg. Chem.* **2014**, *53*, 2361−2363.

DOI: 10.1021/acs.inorgchem.7b01676
Inorg. Chem. 2017, 56, 10706−10716

(29) Nava, A.; Rigamonti, L.; Zangrando, E.; Sessoli, R.; Wernsdorfer, W.; Cornia, A. Redox-Controlled Exchange Bias in a Supramolecular Chain of Fe_4 Single-Molecule Magnets. *Angew. Chem., Int. Ed.* **2015**, *54*, 8777−8782.
(30) Bruker-AXS: Madison, WI, USA, 2013.
(31) (a) Van Der Sluis, P.; Spek, A. L. BYPASS: An effective method for the refinement of crystal structures containing disordered solvent regions. *Acta Crystallogr., Sect. A: Found. Crystallogr.* **1990**, *46*, 194−201. (b) Spek, A. L. PLATON SQUEEZE: A tool for the calculation of the disordered solvent contribution to the calculated structure factors. *Acta Crystallogr., Sect. C: Struct. Chem.* **2015**, *71*, 9−18.
(32) Spek, A. L. Structure validation in chemical crystallography. *Acta Crystallogr., Sect. D: Biol. Crystallogr.* **2009**, *65*, 148−155.
(33) MAGNET, Davidson, E. R. Indiana University, Bloomington, IN, 1999.
(34) (a) Eppley, H. J.; Tsai, H.-L.; de Vries, N.; Folting, K.; Christou, G.; Hendrickson, D. N. *J. Am. Chem. Soc.* **1995**, *117*, 301−317. (b) Soler, M.; Chandra, S. K.; Ruiz, D.; Davidson, E. R.; Hendrickson, D. N.; Christou, G. A third isolated oxidation state for the Mn_{12} family of single-molecule magnets. *Chem. Commun.* **2000**, 2417−2418.
(35) See the Supporting Information.
(36) (a) Sun, Z.; Ruiz, D.; Dilley, N. R.; Soler, M.; Ribas, J.; Folting, K.; Maple, M. B.; Christou, G.; Hendrickson, D. N. The origin of the second relaxation process in the $[Mn_{12}O_{12}(O_2CR)_{16}(H_2O)_4]$ single-molecule magnets: "Jahn−Teller isomerism" in the $[Mn_{12}O_{12}]$ core. *Chem. Commun.* **1999**, 1973−1974. (b) Soler, M.; Wernsdorfer, W.; Sun, Z.; Huffman, J. C.; Hendrickson, D. N.; Christou, G. Single-molecule magnets: Control by a single solvent molecule of Jahn−Teller isomerism in $]Mn_{12}O_{12}(O_2CCH_2Bu^t)_{16}(H_2O)_4]$. *Chem. Commun.* **2003**, 2672−2673.
(37) Wemple, M. W.; Tsai, H.-L.; Folting, K.; Hendrickson, D. N.; Christou, G. Distorted cubane $[Mn_4O_3Cl]^{6+}$ complexes with arenecarboxylate ligation: Crystallographic, magnetochemical and spectroscopic characterization. *Inorg. Chem.* **1993**, *32*, 2025−2031.
(38) Myers, B. E.; Berger, L.; Friedberg, S. Low-temperature magnetization of $Cu(NO_3)_2{\cdot}2.5H_2O$. *J. Appl. Phys.* **1969**, *40*, 1149−1151.
(39) O'Connor, C. J. Magnetochemistry—Advances in theory and experimentation. *Prog. Inorg. Chem.* **1982**, *29*, 203−283.
(40) Sessoli, R.; Tsai, H.-L.; Schake, A. R.; Wang, S.; Vincent, J. B.; Folting, K.; Gatteschi, D.; Christou, G.; Hendrickson, D. N. High-Spin Molecules: $[Mn_{12}O_{12}(O_2CR)_{16}(H_2O)_4]$. *J. Am. Chem. Soc.* **1993**, *115*, 1804−1816.
(41) (a) Aubin, S. M. J.; Sun, Z.; Eppley, H. J.; Rumberger, E. M.; Guzei, I. A.; Folting, K.; Gantzel, P. K.; Rheingold, A. L.; Christou, G.; Hendrickson, D. N. Single-molecule magnets: Jahn−Teller isomerism and the origin of two magnetization relaxation processes in Mn_{12} complexes. *Inorg. Chem.* **2001**, *40*, 2127−2146. (b) Aubin, S. M. J.; Sun, Z.; Rumberger, E. M.; Hendrickson, D. N.; Christou, G. Single-molecule magnets: High-frequency electron paramagnetic resonance study of two isomeric forms of an Mn_{12} molecule. *J. Appl. Phys.* **2002**, *91*, 7158−7160.
(42) Chakov, N. E.; Lee, S.-C.; Harter, A. G.; Kuhns, P. L.; Reyes, A. P.; Hill, S. O.; Dalal, N. S.; Wernsdorfer, W.; Abboud, K. A.; Christou, G. The properties of the $[Mn_{12}O_{12}(O_2CR)_{16}(H_2O)_4]$ single-molecule magnets in truly axial symmetry: $[Mn_{12}O_{12}(O_2CCH_2Br)_{16}(H_2O)_4]{\cdot}4CH_2Cl_2$. *J. Am. Chem. Soc.* **2006**, *128*, 6975−6989.
(43) Wernsdorfer, W. Classical and quantum magnetization reversal studies in nanometer-sized particles and clusters. *Adv. Chem. Phys.* **2001**, *118*, 99−190.
(44) Wernsdorfer, W.; Murugesu, M.; Christou, G. *Phys. Rev. Lett.* **2006**, *96*, 057208.
(45) Vinslava, A.; Tasiopoulos, A. J.; Wernsdorfer, W.; Abboud, K. A.; Christou, G. Molecules at the quantum−classical nanoparticle interface: giant Mn_{70} single-molecule magnets of ∼4 nm diameter. *Inorg. Chem.* **2016**, *55*, 3419−3430.
(46) Wriedt, M.; Yakovenko, A. A.; Halder, G. J.; Prosvirin, A. V.; Dunbar, K. R.; Zhou, H.-C. Reversible Switching from Antiferro- to Ferromagnetic Behavior by Solvent-Mediated, Thermally-Induced Phase Transitions in a Trimorphic MOF-Based Magnetic Sponge System. *J. Am. Chem. Soc.* **2013**, *135*, 4040−4050.
(47) Maspoch, D.; Ruiz-Molina, D.; Wurst, K.; Domingo, N.; Cavallini, M.; Biscarini, F.; Tejada, J.; Rovira, C.; Veciana, J. A nanoporous molecular magnet with reversible solvent-induced mechanical and magnetic properties. *Nat. Mater.* **2003**, *2*, 190−195.

DOI: 10.1021/acs.inorgchem.7b01676
Inorg. Chem. 2017, 56, 10706−10716